Geometric Mechanics of Curved Crease Origami

Marcelo A. Dias,[1,*] Levi H. Dudte,[2,†] L. Mahadevan,[3,‡] and Christian D. Santangelo[1,§]

[1]*Department of Physics, University of Massachusetts Amherst, Amherst, Massachusetts 01002, USA*
[2]*Engineering and Applied Sciences, Harvard University, Cambridge, Massachusetts 02138, USA*
[3]*Physics and Engineering and Applied Sciences, Harvard University, Cambridge, Massachusetts 02138, USA*

(Received 4 June 2012; revised manuscript received 16 August 2012; published 13 September 2012)

Folding a sheet of paper along a curve can lead to structures seen in decorative art and utilitarian packing boxes. Here we present a theory for the simplest such structure: an annular circular strip that is folded along a central circular curve to form a three-dimensional buckled structure driven by geometrical frustration. We quantify this shape in terms of the radius of the circle, the dihedral angle of the fold, and the mechanical properties of the sheet of paper and the fold itself. When the sheet is isometrically deformed everywhere except along the fold itself, stiff folds result in creases with constant curvature and oscillatory torsion. However, relatively softer folds inherit the broken symmetry of the buckled shape with oscillatory curvature and torsion. Our asymptotic analysis of the isometrically deformed state is corroborated by numerical simulations that allow us to generalize our analysis to study structures with multiple curved creases.

DOI: 10.1103/PhysRevLett.109.114301 PACS numbers: 46.70.−p, 46.32.+x, 62.20.mq

Over the last few decades, origami has evolved from an art form into a scientific discipline, where folding techniques have been widely applied to fields of engineering, architecture, and design [1–4], made possible in large part by methods for the mathematical analysis of folded surfaces. Although there are artistic and technological precedents for folding paper along curves [5–10], as seen in Japanese paper boxes and the ubiquitous box for fries, how these geometrical structures get their physical shape is poorly understood, so that the potential associated with curve folding for constructing (quasi)isometric structures using real materials and corrugated shells [11,12] is still only poorly tapped. In this Letter, we consider the geometry and mechanics of the simplest case of a curved fold: an annular elastic sheet folded along a closed, circular curve that buckles out of the plane to resolve a fundamental incompatibility between the folded geometry and the ensuing mechanical stresses.

Qualitative experiments with a complete circular annulus of paper having a concentric, circular crease show that folding buckles the crease into a saddle [Fig. 1(a)], while the same crease along a cut annulus remains planar [Fig. 1(b)]. This behavior is a consequence of a fundamental incompatibility between the geometry of the fold and the stretching elasticity of the sheet. As we will see, and as apparent in Fig. 1(b), the sheet responds to folding by wrapping around itself to eliminate in-plane mechanical stresses. The closed annulus, on the other hand, can relax these stresses by buckling. In the limit of the sheet where the thickness is much smaller than the width, which is itself smaller than the length of the crease, the shape that arises is a balance between the bending energy of the sheets on either side of the crease, the energy at the crease itself, and the geometrical constraints arising from the sheet's closed topology, similar to that seen in the mechanics of strips [13], shells [14], and non-Euclidean objects [15].

We consider an annulus of uniform thickness $t$and width $2w$ folded along a central circular crease of radius r ($t \ll w < r$). In the deformed state, the crease is a space curve parametrized by arc length s, with curvature $\kappa(s)$ and torsion $\tau(s)$, and the surfaces on either side of it come together at a finite fold (or dihedral) angle $\theta(s)$. Assuming isometric deformations away from the crease, the midsurface of the sheet on either side of the crease is developable. Then any point on it can be characterized in terms of a set of

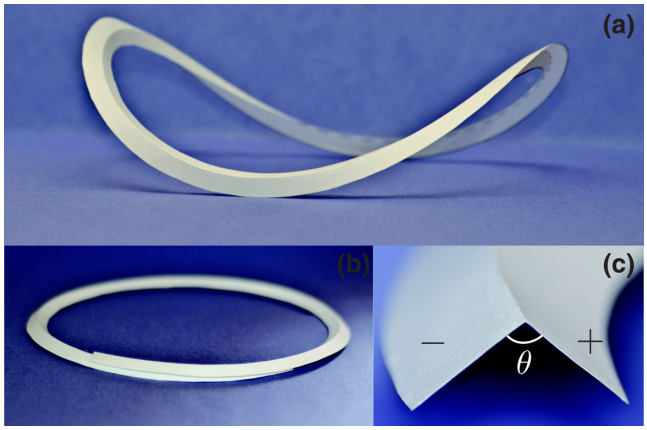

FIG. 1 (color online). A photograph of the model built by cutting a flat annulus of width $2w$ from a flat sheet of paper with central circle of radius r. (a) Folding along its center line buckles the structure out of plane. However, if we cut the annulus, (b), the structure collapses to an overlapping planar state, with curvature given by Eq. (1). (c) The inset shows a cross section of the fold, where the right and the left planes, $\mathbf{X}_+$ and $\mathbf{X}_-$, define the dihedral angle θ.

coordinates (s, v), corresponding to the arc length and the generators of the developable surface on the inside and outside of the crease, $\mathbf{g}_\pm$ [see Fig. 1(c)], with the coordinates $\mathbf{X}_\pm(s, v) = \mathbf{X}(s, 0) + v\mathbf{g}_\pm(s)$. For developable surfaces, the generators must also satisfy the condition that $\mathbf{g}_\pm(s) \times d\mathbf{g}_\pm(s)/ds$ is perpendicular to the crease [16]. Since folding does not induce in-plane strains, the projection of the crease curvature onto the tangent plane on either side of the sheet must remain $1/r$. This leads to two geometrical conditions [8] that relate the dihedral angle of the crease to its spatial curvature and the angle of the generators of the developable surface on either side of it. They read

$$\sin\left(\frac{\theta}{2}\right) = \frac{1}{\kappa}, \tag{1}$$

$$\cot\gamma_\pm = -\frac{1}{2}\left(2\tau \pm r\frac{d\theta}{ds}\right)\tan\left(\frac{\theta}{2}\right), \tag{2}$$

where κ/r and τ/r are the curvature and torsion of the crease, respectively, and $\gamma_\pm$ is the angle between the unit tangent vector of the crease $d\mathbf{X}(s)/ds$ and the generator. We see that $\kappa(s) \geq 1$, with equality only when $\theta = \pi$. For a circular crease concentric with a circular annulus of constant dimensionless half-width $\omega = w/r$, we find

$$v_\pm^{\max}(\xi) = \pm\sin\gamma_\pm(\xi) \mp \sqrt{\omega^2 \mp 2\omega + \sin^2\gamma_\pm(\xi)} \tag{3}$$

to be the dimensionless distance to the boundary along a generator leaving the crease from a point labeled by the dimensionless arc length $\xi = s/r$.

The energy of the sheet is the sum of the energy of deforming the sheet on either side of the crease and that of the fold that connects them. Since the creased folded surface is piecewise developable, the energy per unit surface is proportional to the square of the mean curvature [17]. The mean curvature on either side of the sheet is

$$H_\pm(\xi, v) = \frac{\pm\cot(\theta/2)\csc\gamma_\pm}{2r[\sin\gamma_\pm \mp v(1 \pm \gamma'_\pm)]}, \tag{4}$$

where $(.)' = d/d\xi(.)$. Then the energy of each surface $E_b = B\int_0^{2\pi}\int_0^{v_\pm^{\max}} H_\pm^2 dv d\xi$, where B is the bending stiffness of the material of the sheet. Carrying out the integral along the generators, v, explicitly leads to the following scaled bending energy for the two surfaces:

$$\frac{E_b}{B} = \frac{1}{8}\int_0^{2\pi} d\xi \sum_\pm \frac{\cot^2(\theta/2)\csc^2\gamma_\pm}{1 \pm \gamma'_\pm} \times \ln\left[\frac{\sin\gamma_\pm}{\sin\gamma_\pm - v_\pm^{\max}(\xi)(1 \pm \gamma'_\pm)}\right]. \tag{5}$$

We see that Eq. (5) is determined entirely in terms of the geometry of the crease. To model the fold itself, we use a phenomenological energy functional measuring the deviation of $\theta(\xi)$ from an equilibrium angle θ_0, which we assume to be constant, so that the scaled crease energy is as follows:

$$\frac{E_c}{B} = \frac{\varsigma}{2}\int_0^{2\pi} d\xi\left[\cos\left(\frac{\theta(\xi)}{2}\right) - \cos\left(\frac{\theta_0}{2}\right)\right]^2, \tag{6}$$

where $\varsigma = Kr/B$ is the ratio of the crease stiffness K and the bending stiffness B. This energy reduces to a simple quadratic expression in the difference $\theta - \theta_0$ when $\theta \sim \theta_0$; although the precise form of this term does not affect our analytic results, it conforms to our numerical model [18].

The equilibrium shape of the curved crease results from minimizing $E = E_b + E_c$ and is characterized by three parameters: the scaled natural width of the ribbon ω, the natural dihedral angle between the two surfaces adjoining the crease θ_0 and the dimensionless crease-surface energy scale ς, subject to appropriate boundary conditions. For example, an open circular crease has free ends and thus prefers to remain planar with $\tau = 0$, since nonplanarity would increase both the curvature and torsion (see Supplemental Material [19]). A closed crease, however, is frustrated by geometry, forcing it to buckle, a fact that follows from the inequality $\kappa = 1/\sin(\theta/2) > 1$ when $\theta < \pi$, which requires $\int d\xi\kappa > 2\pi$, and is incompatible with a planar crease with $\tau = 0$ [8].

Although geometrical constraints induce buckling, the resulting fold shapes are determined by minimizing the total elastic energy consisting of contributions from the sheet [Eq. (5)] and the fold [Eq. (6)], expressed entirely in terms of the curvature and torsion of the crease [13,20]. For relatively narrow but stiff folds, i.e., $\omega \ll 1$ and $\varsigma \gg 1$ are weakly folded, the dihedral angle $\theta_0 \sim \pi$, and hence $\epsilon \equiv 1/\sin(\theta_0/2) - 1 \ll 1$. Then, we find that the total scaled energy $E = (E_b + E_c)/B$ simplifies to (see Supplemental Material [19])

$$E \approx \int_0^{2\pi} d\xi\left\{\frac{\varsigma}{4\epsilon}\left(\kappa - 1 - \epsilon\right)^2 + \frac{\omega}{2}\tau^2\right\} \tag{7}$$

in terms of the scaled curvature κ and torsion τ. We see that as $\varsigma \to \infty$, the rescaled curvature $\kappa \to 1/\sin(\theta_0/2) = 1 + \epsilon$, the prescribed curvature. The minimal energy crease shape, therefore, minimizes τ^2 subject to the constraints of fixed length and curvature. In this limit, the Euler-Lagrange equations become $[\tau'' + (1 + \epsilon)^2\tau]' \approx 0$ at constant curvature (see Supplemental Material [19]). If $\epsilon = 0$, corresponding to a dihedral angle $\theta_0 = \pi$, the solution to these equations is infinitely smooth. Otherwise, a solution of continuity class C^4 may be obtained to these equations with $\kappa = 1 + \epsilon$ and oscillating torsion

$$\delta\tau = \begin{cases} \tau_0\left[1 - \frac{\cos[(\xi - \pi/2)(1+\epsilon)]}{\cos[(\pi/2)(1+\epsilon)]}\right], & 0 \leq \xi \leq \pi \\ -\tau_0\left[1 - \frac{\cos[(\xi - 3\pi/2)(1+\epsilon)]}{\cos[(\pi/2)(1+\epsilon)]}\right], & \pi \leq \xi \leq 2\pi. \end{cases} \tag{8}$$

The absolute magnitude of the torsion τ_0 is then determined by the condition that the curved fold has an arc length $2\pi r$, and consistent with the four-vertex theorem for closed

convex space curves, there are four points with vanishing torsion [21].

To go further, we can carry out an asymptotic analysis of the Euler-Lagrange equations obtained by minimizing $E = E_b + E_c$; this must be performed by expanding the shape of the crease around a planar curve of constant curvature, κ_0. Following Refs. [13,20], we write $\kappa = \kappa_0 + \delta\kappa$ and $\tau = \delta\tau$ and compute the Euler-Lagrange equations. To lowest order, we obtain an algebraic expression determining the ideal curvature of the crease κ_0 for arbitrary ς, ϵ, and ω (see Supplemental Material [19]), the curvature of an incomplete or severed planar annular fold with zero torsion. To next order, we find that both the curvature and torsion oscillate; a typical analytical solution is shown in Fig. 2(a), with the inset showing the oscillating torsion vanishing at the extrema of the curvature (see Fig. 1). Here, the overall amplitude of τ is chosen to close

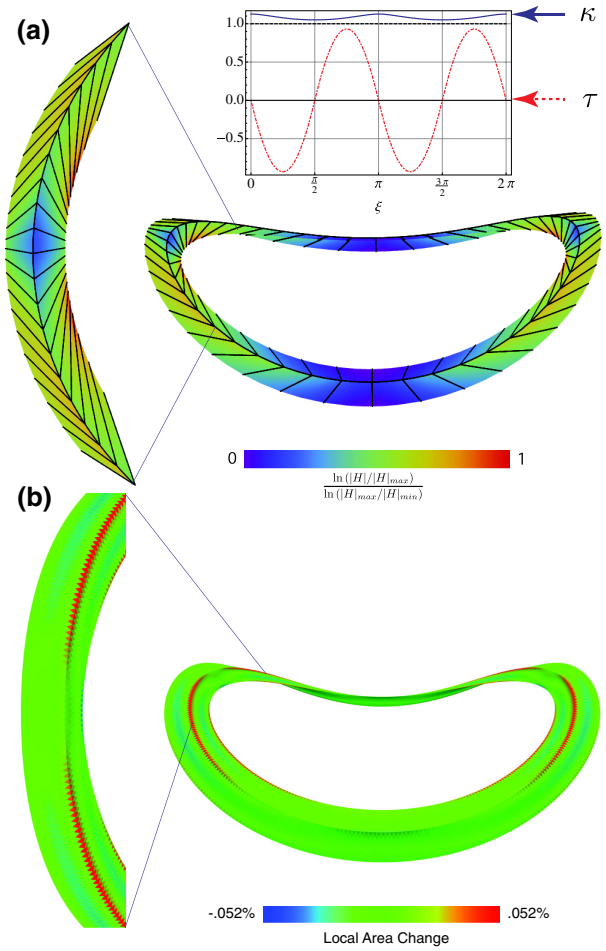

FIG. 2 (color online). (a) Perturbative fold of width $\omega = 0.1$ and $\varsigma = 2/\sqrt{3}$ shaded by mean curvature. The generators are indicated by the lines on the surface. The inset shows the dimensionless torsion and curvature of the crease. (b) A simulated fold of width $\omega \approx .0994$ shaded by local area change relative to the flat state.

the curve, with $\theta(0)$ and $\theta(\pi/2)$ parametrizing the solutions (see Supplemental Material [19]).

These qualitative features are also confirmed by direct numerical minimization of the energy of a triangular mesh model for the curved origami structure, in which each edge is treated as a linear spring, with the stretching stiffness inversely proportional to rest length. We apply restorative bending forces to the adjacent triangles in each sheet so that they prefer collinear normals, with the scaled ratio of the bending stiffness to the stretching stiffness $B/Sl^2 \approx 10^{-6}$. Adjacent triangles that straddle the crease prefer a fixed, nonplanar dihedral angle [18] (see SI). The presence of a small but finite extensibility of this model implies that our simulations relax the isometry of the folding process and thus allow us to capture how the extension and shear arise in wide folds [Fig. 2(b)]. We find that the extensional and shear strains typically localize where the mean curvature becomes large, consistent with our isometric analytic theory [shown in Fig. 2(a)].

Moving beyond the simple asymptotic theory for narrow folds, we consider the dependence of the solution on the scaled width by using the perturbative shapes as a variational ansatz in the exact expression for the energy $E_b + E_c$. Since the shapes have a fourfold symmetry, we expect to see a coincidence between $\theta(0)$ and $\theta(\pi/2)$. In Fig. 3(a), we plot $|\theta(0) - \theta(\pi/2)|$ for the minimal energy configuration as a function of the scaled width ω. We see that when $\omega \lesssim 0.1$, annuli with large ς have a nearly constant dihedral angle around the entire length of the fold, with $\theta(0) \approx \theta(\pi/2)$ for the narrowest fold widths. However, for small ς, the energy minimum generically has $\theta(0) \neq \theta(\pi/2)$; this discrepancy increases with the scaled width ω. Plotting the corresponding energy landscape in Figs. 3(b)–3(d) for some representative values of ω, we see that the energy contours develop forks, because the range of $\theta(0)$ and $\theta(\pi/2)$ are forbidden by the geometric constraints that the generators of our two surfaces can intersect only outside the actual surface, else the bending energy diverges.

To avoid the intersection of generators inside the outer surface, it is required that

$$\gamma'_+ < \frac{\sin\gamma_+}{v_+^{\max}} - 1 \quad \text{and} \quad \gamma'_- > -\frac{\sin\gamma_-}{v_-^{\max}} + 1, \tag{9}$$

which expression reduces to $|\tau'| < (1-\omega)\cot(\theta/2)/\omega$ at the points where $\tau = 0$. Similarly, to avoid the intersection of the generators on the inner surface inside the inner boundary requires the discriminant in Eq. (3) to be positive, implying a bound on the torsion,

$$\left|\tau + \frac{\theta'}{2}\right| < \frac{1-\omega}{\sqrt{2\omega - \omega^2}} \cot\left(\frac{\theta}{2}\right). \tag{10}$$

These geometrical bounds restrict the range of allowed torsion and thus the buckling of the crease. As a consequence, wide folds will become resistant to deformations as the sheet quickly reaches a regime where the generators

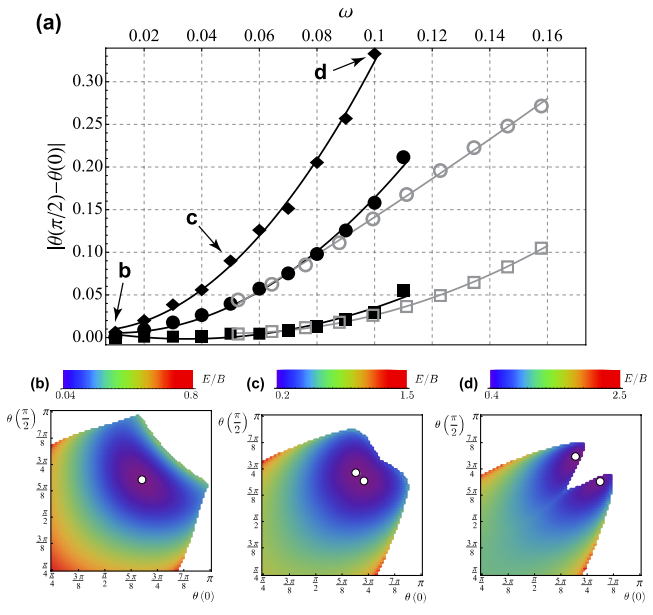

FIG. 3 (color online). (a) Angle differences $|\theta(\pi/2) - \theta(0)|$ as a function of ω with $\theta_0 = 2\pi/3$. The curve with diamonds are computed from the first-order perturbation theory with $\varsigma = 2/\sqrt{3}$ and $\theta_0 = 2\pi/3$. The numerical simulations are shown in gray with $\varsigma = 2\sqrt{3}$ (open circles) and $\varsigma = 160/\sqrt{3}$ (open squares), and are compared with nonperturbative variational ansatz, $\kappa_{(2)}$ and $\tau_{(2)}$, described in the text with $\varsigma = \sqrt{3}/40$ (circles) and $\varsigma = \sqrt{3}/2$ (squares). Corresponding energy landscapes, as a function of $\theta(0)$ and $\theta(\pi/2)$, respectively, are shown for (b) $\omega = 0.01$, (c) 0.05, and (d) 0.1, with energy minima drawn as white dots.

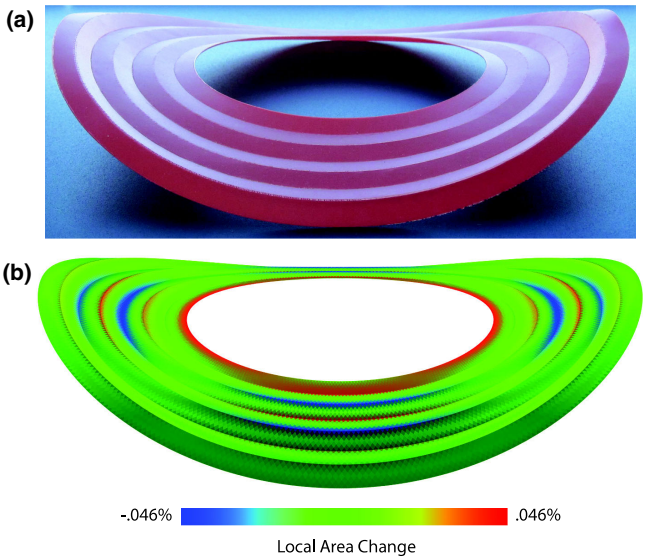

FIG. 4 (color online). (a) A plastic model of six circular folds generated by perforating the folds at equal intervals with a laser cutter. The ratio of outer to inner boundary is 2. (b) A simulation result with the same planar geometry as the plastic model shaded by local area change. Multiple fold simulation has the same magnitude order of area change as that of single fold simulation and agrees visually with the physical model in (a).

start to nearly intersect in the neighborhood of $\xi = \pi/2$. In Fig. 3(d), this is manifested by the presence of large forks carved out by the forbidden configurations. Since energy minima occur close to the singularities, our perturbative expansion of the shape is approximate at best. However, even at intermediate widths, where the perturbative expansion should be at least qualitatively valid, bifurcation of the minima show up in the shadows of the prominent forks observed in Fig. 3(d).

These calculations suggest a second improved ansatz: $\kappa_{(2)} = \kappa_0 + \kappa_1 \cos(2\xi)$ and $\tau_{(2)} = \tau_0[\sin(2\xi) + \eta \sin(4\xi)]$, choosing τ_0 to close the fold and η to minimize the energy. When $\eta = 0$, we now find very good agreement with the perturbative ansatz previously considered. However, we find that $\eta \approx -0.45$ for large widths, which lowers the maximum of the torsion and better satisfies the singularity bounds in Eqs. (9) and (10). Using ς as a fitting parameter, we see that $\theta(\pi/2) - \theta(0)$ agrees quite well with the numerical solutions for small ω and only diverges from numerical simulations for large widths around $\omega \sim 0.08$, as shown in Fig. 3(a).

Finally, we consider structures built from multiple, concentric folds (Fig. 4). Again, the large penalty for stretching leads to strong geometric constraints connecting the curvature and torsion of the crease to the dihedral angle of the fold given by Eq. (1), leading to self-similar creases and folds. The generator on the outside of a crease must coincide with the generator on the inside of the next crease, fixing the angle γ_+ on the inside of the next crease, while the torsion determines the relationship between γ_+ and γ_-, so that the direction of the next set of generators emerges. This procedure follows from the first crease to the last crease, until we reach a boundary or the generators cross. Our numerical simulations confirm this and further show that multiple creases stretch very little and do buckle rigidly.

Our study of curved crease origami shows that a consequence of the fundamental frustration between folding along a curve and the avoidance of singularities and in-plane stretching imposes geometric constraints on the shape that are reflected in a bifurcation of the curvature of a closed crease of large width. Indeed, the coupling between shape and in-plane stretching endows these structures with a stiffness and response that is unusual, as we have demonstrated in the simplest of situations—a closed circular fold. Moving forward, our approach may be generalized to more complex curves having variable dihedral angles in folded structures with curved creases, and thus sets the stage for the analysis and design of these objects.

We thank Tom Hull and Pedro Reis for discussions, Badel Mbanga for help with photography, and NSF DMR 0846582, the NSF-supported MRSEC on Polymers at UMass (DMR-0820506) (M. D., C. S.), the Wyss Institute for Bioinspired Engineering (L. D., L. M.), and the MacArthur Foundation (L. M.) for support.

*madias@physics.umass.edu
†ldudte@seas.harvard.edu
‡lm@seas.harvard.edu
§csantang@physics.umass.edu

[1] K. Miura, in *Method of Packing and Deployment of Large Membranes in Space* (The Institute of Space and Astronautical Science, 1980).
[2] E. Demaine and P. ORourke, *Geometric Folding Algorithms* (Cambridge University, Cambridge, England, 2009).
[3] E. Hawkes, B. An, N. M. Benbernou, H. Tanaka, S. Kim, E. D. Demaine, D. Rus, and R. J. Wood, Proc. Natl. Acad. Sci. U.S.A. **107**, 12441 (2010).
[4] M. Schenk and S. D. Guest, in *Origami Folding: A Structural Engineering Approach, Origami 5*, edited by Mark Yim (A K Peters Ltd, Wellesley, MA, 2011).
[5] H. M. Wingler, *Bauhaus: Weimar, Dessau, Berlin, Chicago* (MIT, Cambridge, MA, 1969).
[6] D. A. Huffman, IEEE Trans. Comput. **C-25**, 1010 (1976).
[7] J. P. Duncan and J. L. Duncan, Proc. R. Soc. A **383**, 191 (1982).
[8] D. Fuchs and S. Tabachnikov, Am. Math. Mon. **106**, 27 (1999).
[9] H. Pottmann and J. Wallner, *Computational Line Geometry* (Springer-Verlag, Berlin, 2001).
[10] M. Kilian, S. Flöry, Z. Chen, N. J. Mitra, A. Sheffer, and H. Pottmann, ACM Trans. Graph. **27**, 1 (2008).
[11] J. P. Duncan, J. L. Duncan, R. Sowerby, and B. S. Levy, Sheet Metal Industries **58**, 527 (1981).
[12] K. A. Seffen, Phil. Trans. R. Soc. A **370**, 2010 (2012).
[13] E. L. Starostin and G. H. M. van der Heijden, Phys. Rev. E **79**, 066602 (2009).
[14] B. Audoly and Y. Pomeau, *Elasticity and Geometry: From Hair Curls to the Nonlinear Response of Shells* (Oxford University, New York, 2010).
[15] C. D. Santangelo, Europhys. Lett. **86**, 34003 (2009).
[16] M. P. do Carmo, *Differential Geometry of Curves and Surfaces* (Prentice-Hall, Englewood Cliffs, NJ, 1976).
[17] A. E. H. Love, *A Treatise on the Mathematical Theory of Elasticity* (Dover, New York, 1944).
[18] R. Bridson, S. Marino, and R. Fedkiw, *ACM SIGGRAPH/ Eurographics Symposium on Computer Animation (SCA), 2003*, pp. 28–32.
[19] See Supplemental Material at http://link.aps.org/supplemental/10.1103/PhysRevLett.109.114301 for a derivation of the fold energy and analytical perturbation theory.
[20] R. Capovilla, C. Chryssomalakos, and J. Guven, J. Phys. A **35**, 6571 (2002).
[21] V. D. Sedykh, Bull. Lond. Math. Soc. **26**, 177 (1994).